Technical report

Action of Hydraulic Pressure on Portland Cement Mortars - Current Understanding and Related Progress of the First-Ever In-Situ Deep Sea Tests at a 3515 m Depth

Keisuke Takahashi[1*], Yuichiro Kawabata[2], Mari Kobayashi[3], Shinpei Gotoh[4], Shun Nomura[5], Takafumi Kasaya[6] and Mitsuyasu Iwanami[7]

Received 15 February 2021, accepted 11 March 2021 doi:10.3151/jact.19.226

Abstract

In order to realize the utilization of cement-based materials in the special extreme environment, the deep sea, the authors have launched a project targeted at creating a technology platform with in-situ methods and systems for monitoring and evaluating cement-based materials located at deep ocean bottom sites. The first in-situ test in the world with a view to investigating the time-dependence of the volumetric stability and microstructure of Portland cement mortar following its long-term exposure to deep-sea conditions is currently underway at a 3515-m depth in the Nankai Trough. This paper reviews previous studies about the influences of deep-sea hydraulic pressure on cement-based materials, verifies the action of short-term hydraulic pressure using Portland cement mortars on a laboratory scale, and introduces the ongoing progress of in-situ deep-sea tests. Results from laboratory tests indicate that dimensional changes were provoked by liquid water infiltration and confinement while under short-term hydraulic pressure, however, time-dependent behavior under stresses such as creep has not appeared. Weight gain, changes in pore-size distribution, compressive strength and bending strength of the cement mortar were monitored after pressurization and depressurization processes.

1. Introduction

Defined as a marine environment at a water depth greater than 200 m (Danovaro *et al*. 2017), the deep sea is referred to as the *last frontier* and has attracted much research attention within the fields of natural science and resource development (Araki *et al*. 2017; Ramirez and Billet 2006; Sharma 2015; Miller *et al*. 2018). Carbon dioxide capture and storage under the seafloor (Hume 2018) and underwater structures in which the occupants live and work (Shimizu Corporation n.d.) could lead to technological breakthroughs in utilizing marine areas. Recently for advancement of the field of cutting-edge physics, an undersea research infrastructure that will house the next generation neutrino telescopes KM3NeT is being constructed in the Mediterranean Sea (Margiotta 2014; Le Breton 2019). In Japan, the construction of an ocean bottom detector with the size of 10–50 kt at sea depths of 1000 to 5000 m is being planned for imaging the deep mantle structure by geoneutrino observation (Sakai *et al*. 2020). In order to realize these pioneering and innovative projects, the establishment of infrastructures in deep-sea environments will be required, where physicochemical conditions differ extremely from land and shallow-sea areas. Assuming these applications will be developed, construction materials would be required to maintain their robustness for a very long period (millennial scale).

Cement is widely used as a construction material due to its versatility and its ability to resist destruction, wear and environmental impacts. It has already been utilized in shallow-sea areas at depths of ca. 20 m to construct embankments, piers and breakwaters. The durability of cement-based materials in shallow-sea environments have been investigated during the last 50 years, and the deterioration process has been almost clarified (Mather 1964; Gjorv 1971; Metha 1990; Mohammed *et al*. 2003; De Weerdt *et al*. 2014; Jakobsen *et al*. 2016). The durability of the cement-based materials under deep-sea conditions, however, has hardly been reported, although these materials could be applied in the future construction of infrastructures in deep-sea areas.

Very specific to deep seas are environmental condi-

[1]Chief researcher, Technical Development Center, Ube Industries, Ltd., 1-6 Okinoyama Kogushi, Ube, 7558633, Japan. *Corresponding Author,
E-mail: Keisuke.Takahashi@ube-ind.co.jp
[2]Head of Frontier Technologies for Structures Group, Structural Engineering Field, Port and Airport Research Institute, National Institute of Maritime, Port and Aviation Technology.
[3]Researcher, Technical Development Center, Ube Industries, Ltd.
[4]Assistant professor, Department of Marine Electronics and Mechanical Engineering, Tokyo University of Marine Science and Technology.
[5]Technical researcher, Department of Mathematical Science and Advanced Technology, Japan Agency for Marine-Earth Science and Technology.
[6]Group leader, Research Institute for Marine Resources Utilization Submarine Resources Research Center, Japan Agency for Marine-Earth Science and Technology.
[7]Professor, Department of Civil and Environmental Engineering, Tokyo Institute of Technology.

tions such as high hydraulic pressure and constant low temperature where carbonates become more soluble in seawater and pH is decreased slightly. Such specific environments have impacts on the durability of cement-based materials. The authors have reported that significant deterioration was observed in a Portland cement mortar exposed 608 days to a seafloor environment at a depth of 1680 m at Tarama Knoll and interpreted that a key influencing factor for the disintegration of the mortar specimen could be extremely low temperature (Kobayashi *et al*. 2021). Although the effect of high hydraulic pressure has been rarely addressed in our previous paper, hydraulic pressure could be another key influencing factor that can affect the durability of the mortar under the deep-sea environment. There are some studies focused on the influences of hydraulic pressure on cement-based materials.

From the backgrounds above, action of hydraulic pressure on cement-based materials remains controversial. In Section 2, these works are reviewed, and current understanding is shown. The distinction between underwater pressures such as hydrostatic and other changing pressures is not central to our study, hence we will refer simply to hydraulic pressure in what follows. In Section 3, we investigate the effects of short-term hydraulic pressure on Portland cement mortars during the initial 7 days of submersion under 17 MPa (equivalent to ca. 1700 m in depth) by measuring with X-ray microtomography scanning (X-μCT), and by measuring the strain in the mortar specimen while under hydraulic pressure and the changes in material properties provoked by pressurization and depressurization. Disintegration of the mortar specimen observed in our previous study (Kobayashi *et al*. 2021) is verified from the aspect of hydraulic pressure on a laboratory scale.

Furthermore, in order to grasp the action of long-term and higher hydraulic pressure as well as the real behavior of cement-based materials under actual deep-sea conditions, the authors have set up a project that targets the creation of a technology platform of in-situ deep-sea monitoring methods and the corresponding evaluation of these materials by using the on-site measuring apparatus (Section 4). Within the project, the in-situ test is currently being performed at 3515 m depth in the Pacific Ocean's Nankai Trough in order to investigate the time-dependent volumetric stability and microstructure-related durability issues due to the long-term exposure to seabed. To the best of the authors' knowledge, this is the first-ever in-situ deep-sea test on cement-based materials. The specimen and measurement data that play an essential role in this deep-sea research study will be retrieved in 2021. This paper introduces the progress of the in-situ test and demonstrates the results of the related preliminary testing under 35 MPa of hydraulic pressure using a hyperbaric chamber.

2. Research review: Influences of hydraulic pressure on cement-based materials

Hydraulic pressure can be a key factor in the deterioration of cement-based materials under deep-sea conditions since these materials as a porous medium with micro to macro pores are subjected to hydraulic pressure as well as liquid water infiltration. Several reports indicate that the pressure generates the isotropic confinement and water infiltration, which decreases the compressive strength and bending strength of concrete (Haynes and Rail 1986; Craig *et al*. 1981; Pauli and Clapper 1967), whereas confined concrete results in a strength increase (Mander *et al*. 1988). Fracture behaviors of the cement-based materials under high hydraulic pressure could be dependent on pore volume, size, distribution and tortuosity (Hori *et al*. 2015). **Figure 1** illustrates the rupture of the hardened Portland cement paste with a water-to-cement ratio of 0.60 under high hydraulic pressures. Once the pores in concrete are saturated with infiltrated water, the internal pressure acting on the solid skeleton is released. Spatiotemporal differential release of external and internal pressures at the infiltration boundary could generate strain (Clayton 1998). The fractured surface of columnar and cylindrical specimen can be ellipsoidal in shape.

In 1971, the U.S. Naval Civil Engineering Laboratory in California started to study hollow concrete spheres at ocean depths ranging from 550 m to 1500 m. These spheres had an outside diameter of 1.7 m and a wall thickness of 0.1 m. The concrete mix was designed with a water-to-cement ratio of 0.40. They reported that the compressive strength of cores drilled from the specimens that were submerged for 10 years decreased about 15 % compared to the fog-cured specimens over this time period, and specimens deeper than 1100 m were crushed under the pressure (Haynes *et al*. 1976). The concrete was saturated with seawater, as findings showed that the specimens retrieved after 10 years contained 53 L of seawater inside, which was 3 % of its interior volume (Rail and Wendt 1985). It should be noted that the specimens for those compressive tests were affected by depressurization during the salvage process. Microstructural damages, which could be generated by the water infiltration during pressurization (Wang *et al*. 2016) and/or by the long-duration exposure to deep sea conditions (Rail and Wendt 1985), might be emphasized by the release of water confinement itself (Clayton 1998) and/or the gasified air during depressurization associated with the retrieval of the specimens.

Clayton (1998) measured compressive strength and bending strength of concrete while under hydraulic pressure. The test apparatus consisted of a load cell situated beneath the specimen inside a high-pressure vessel. The concrete mix was designed with water-to-cement ratio of 0.55. In the case that pressure was kept at 60 MPa for 20 h, compressive strength and bending strength while under hydraulic pressure de-

creased about 30% and 50% respectively, compared to the unpressurized condition. Both compressive strength and bending strength remained the same after the following depressurization from 60 MPa to atmospheric pressure (0.1 MPa). When the applied hydraulic pressure was high enough, hydraulic confinement was dominant as the result and permanent damages occurred during the rise and/or sustainment of the high hydraulic pressure. Depressurization back to atmospheric pressure resulted in no further significant damage. In contrast, in the case that the applied pressure is not high, the bending strength while under hydraulic pressure remained the same compared to unpressurized condition even after 6 days of pressurization at 30 MPa, but decreased about 25% after the following depressurization to atmospheric pressure. The damage in this case might be due to the differential release of external and internal pressure as well as the release of the confining stress itself.

An in-situ test was recently carried out in the Arctic Sea at a 2500-m depth that monitored temperature and humidity inside underwater housings made of ultra-high performance concrete in order to determine alternative materials to titanium, special stainless steel and aluminum for housings (Wilhelm and Curbach 2017; ROBEX n.d.). On a laboratory scale, Wilhelm and Curbach (2017) have described that the implosion behavior of concrete housings can be simulated by empirical equations determined by Albertson (1973) modified with a nonlinear material law for concretes, which was calibrated with results from multiaxial strength tests (Hampel *et al.* 2009; Ritter and Curbach 2015).

The previously mentioned strength decrease and implosion behavior could be affected by in-situ dimensional changes, including creep, during long-term exposure to hydraulic pressure as well as instantaneous elastoplastic strain during the diving and pressurizing of the specimen. In order to clarify the behavior of cement-based materials under high hydraulic pressure, in-situ monitoring is required as such an approach has not been reported. In-situ monitoring in deep seas will help to gain data and insights on a real behavior of cement-based materials under deep-sea conditions, which includes pressurization/depressurization. The corresponding mechanisms will also be elucidated.

3. Effects of short-term hydraulic pressure on a laboratory scale – the first step for verifying mechanical damages on the mortar specimens

As already reported in Kobayashi *et al.* (2021), specimens salvaged from the deep seafloor with a depth of 1680 m at Tarama Knoll were severely damaged as shown in **Fig. 2**. We have interpreted that decalcification of portlandite and calcium-silicate hydrates (C-S-H) and the formation of magnesium silicate hydrate, thaumasite and ettringite could be accelerated due to extremely low temperature and can result in the disintegration of the mortar specimen. Although cement mortars are porous medium with microstructure has risks of deformation and cracking under high hydraulic pressure, their behavior is yet poorly understood. Lab tests were therefore performed to investigate the behavior of cement mortar under high hydraulic pressure same with the exposure

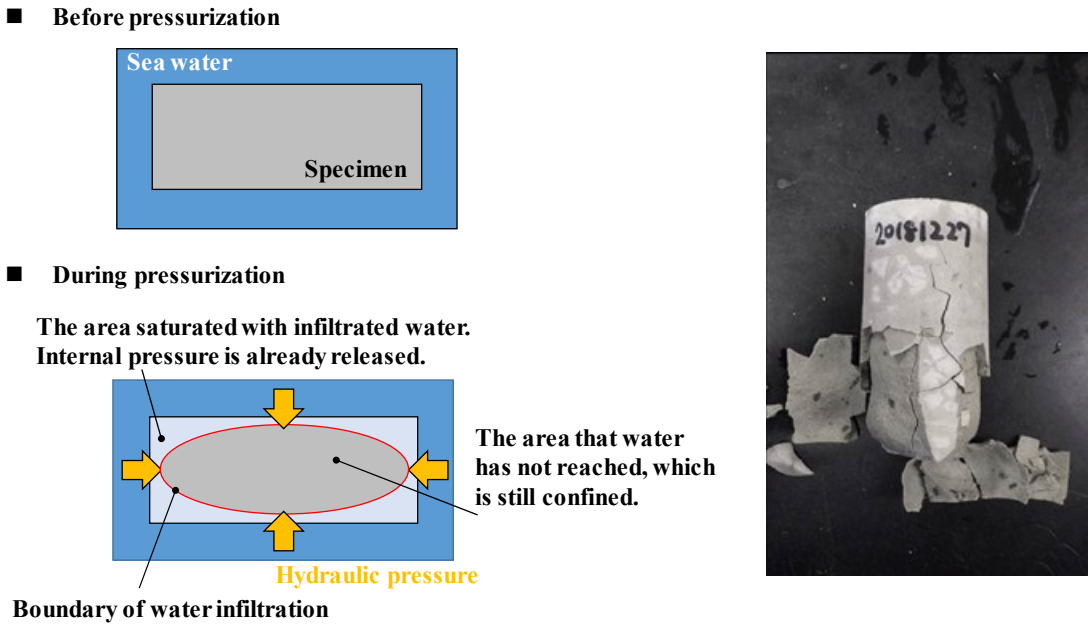

Fig. 1 Illustration of the rupture of the cement-based specimen due to water transport and confinement under high hydraulic pressure (*left*). Hardened Portland cement paste that was pressurized from 0.1 MPa to 60 MPa at a pressurizing rate of 1 MPa/min, and the 60 MPa was maintained for 60 min, then depressurized from 60 MPa to 0.1 MPa at a depressurizing rate of 1 MPa/min (*right*). The original shape of the hardened paste was 50 mm in diameter and 100 mm in height.

Table 1 Mix proportions of the experimental mortars (unit: g).

Mortar	Cement	Sand[a]	PCE	MC	Defoamer	Tap water
A	500	500	4.0	2.4	1.0	300
B	500	500	0.5	1.0	0.1	300

[a]Siliceous sand with a particle size of 0.5–1.0 mm was used for mortar A. Siliceous sand with a particle size of 0.1–2.0 mm, which is standard sand produced by Japan Cement Association, was used for mortar B.

Table 2 Composition of Portland cement measured by X-ray fluorescence (unit: %). LOI: loss on ignition.

SiO_2	Al_2O_3	Fe_2O_3	CaO	MgO	SO_3	Na_2O	K_2O	LOI	Total
20.37	5.26	2.67	65.31	1.19	2.86	0.24	0.28	1.00	99.18

Table 3 Physical properties of mortars A and B. Flow value, air content, compressive strength and bending strength were measured based on JIS R 5201:2015.

Mortar	Flow value (mm)	Air content (%)	Density (g/cm^3)	Compressive strength (N/mm^2)	Bending strength (N/mm^2)
A	295	5.0	2.0	38.4	4.4
B	268	5.0	1.9	34.0	5.8

condition at Tarama Knoll. In this paper the effects of short-term hydraulic pressure is explained. The action of long-term hydraulic pressure is still under measurement and will be published soon.

3.1 Materials and test specimens

The mortar mix A shown in **Table 1** used for laboratory experiments contains Portland cement (PC), siliceous sand, polycarboxylic ether superplasticizer (PCE), methyl cellulose thickener (MC) and defoamer. The composition of PC, measured by X-ray fluorescence according to the Japanese Industrial Standard (JIS R 5304), is shown in **Table 2**. The water-to-cement ratio was 0.60 by reference to the upper limit of 0.65 for this mixing ratio in non-reinforced structures established by Ports and Harbours Bureau, MLIT. *et al*. (2009). The dry mortar mixes were pre-mixed and subsequently mixed with water for 2 min at 700 rpm using a mechanical mixer. Mortar specimens with the size of 40 mm × 40 mm × 160 mm were prepared for the measurement of materials characterization before/after pressurization, strain measurement while under hydraulic pressure and X-μCT after pressurization/depressurization. **Table 3** shows flow value, air content and density of the mortar A immediately after mixing, and compressive and bending strength of the mortar specimen cured for 28 days under sealed conditions. These testing and curing were performed at a constant temperature of 20ºC 65 %RH. Prior to the measurements shown in Section 3.3, the mortar specimens were cured for 28 days under sealed conditions at 20ºC. The variations of the temperature and humidity were ±1ºC and ±5% RH, respectively.

3.2 High-pressure vessel and pressurization protocol

The test apparatus for pressurization is shown in **Fig. 3**. A high-pressure vessel was custom manufactured with an inner diameter of 150 mm and an inner height of 250 mm. The top lid can be fixed to the vessel by tightening bolts. An underwater connector Seacon RMK-6-FS/MP (TE Connectivity Co.) was installed on the lid to connect the cables from the strain gauges and data logger.

The inner container of the high-pressure vessel was filled with saturated lime water in order to avoid decal-

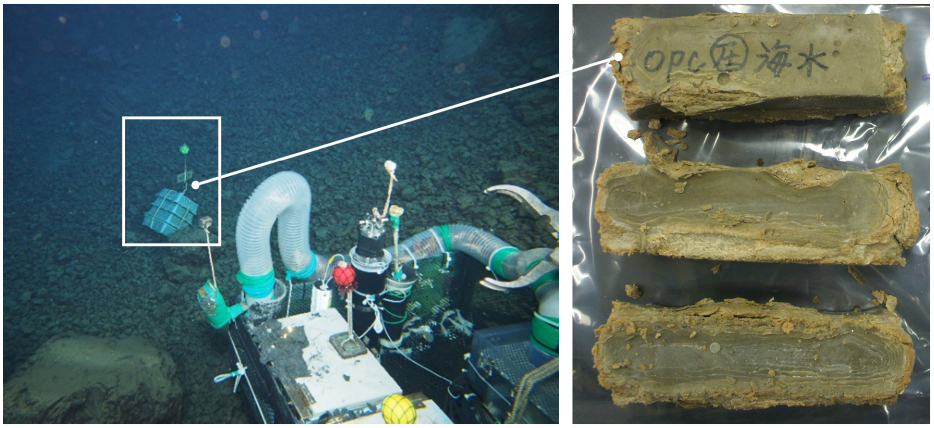

Fig. 2 Mortar specimens exposed to the deep seafloor with a depth of approximately 1,680 m at Tarama Knoll (*left*; this photograph was obtained from JAMSTEC) and the mortar specimens salvaged from Tarama Knoll (*right*).

cification of the mortar specimen. After inserting two specimens and closing the vessel, the hydraulic pressure was increased at a rate of 0.5 MPa/min to 17 MPa for 35 min using a hand pump. The pressure was then kept constant at 17 MPa for a period of 7 days at a maximum. Depressurization was performed by opening the pressure reducing valve manually, which meant the depressurization rate was not controlled. Applied maximum pressure value of 17 MPa and pressurization rate of 0.5 MPa/min simulated the real operation using a deep-submergence research vehicle Shinkai 6500 (JAMSTEC document catalog YK17-17).

3.3 Measurements

Materials characterization was carried out before and after hydraulic pressurization/depressurization. Also, the deformation as well as liquid water infiltration through pores of the cement mortar while under hydraulic pressure were investigated. Every test was repeated more than twice under the same conditions to confirm the reproducibility of measurements.

(1) Strain while under hydraulic pressure

For the specimens dedicated to strain measurement, a strain gauge PML-60 (Tokyo Measuring Instruments Laboratory Co, Ltd.) with the size of 13 mm × 5 mm × 125 mm was embedded in the mortar specimen. Lead wire from the specimens was covered with waterproofing materials and connected to the data logger via the underwater connector from the top lid. Strain was measured continually during the 7 days while applying the hydraulic pressure of 17 MPa.

(2) Pore-size distribution, weight change, compressive strength and bending strength

Differences in materials characterization such as the pore-size distribution, weight, compressive strength and bending strength of the mortar specimens between, before and after periods of hydraulic pressurization were investigated. The mortar specimens were pressurized for periods of 1 day and 7 days. The pore-size distribution was determined via the mercury intrusion porosimetry (MIP) method using AutoPore IV 9500 (Micromeritics Instrument Corporation) porosimeter. The contact angle was set at 140º. The mortar specimens for MIP were cut into 5-mm cubes and the hydration was stopped with isopropanol. Weight change of the specimens before and after pressurization was given as a percentage. Compressive strength and bending strength were measured based on JIS 5201 R: 2015.

(3) X-ray microtomography scanning (X-μCT)

X-μCT was conducted in order to investigate damages on the mortar specimen resulting from short-term water infiltration. The model ScanXmate-D200RSS900 X-μCT (Comscantecno Co., Ltd.) with a maximum voltage of 115 keV and X-ray tube current of 110 μA was used. The transmitted X-rays were detected by a 418 mm by 418 mm flat panel with a resolution of 1504 pixels by 1504 pixels. A radiograph was acquired every 0.3° for a total of 1200 images. The three-dimensional voxel size was 52 μm × 52 μm × 52 μm. Consequently, 1504 slices were generated in each of the vertical and horizontal directions. The durations of pressurization were 30 min, 1 day and 7 days. Tap water was used for this test. After each predetermined duration, the specimen was depressurized and taken out of the vessel. Subsequently, three-dimensional images of X-μCT scans were taken.

3.4 Results and discussions

(1) Deformation and water infiltration of mortar during short-term pressurization

Figure 4 depicts an example of three-dimensional images of X-μCT scans before and after pressurization for 1

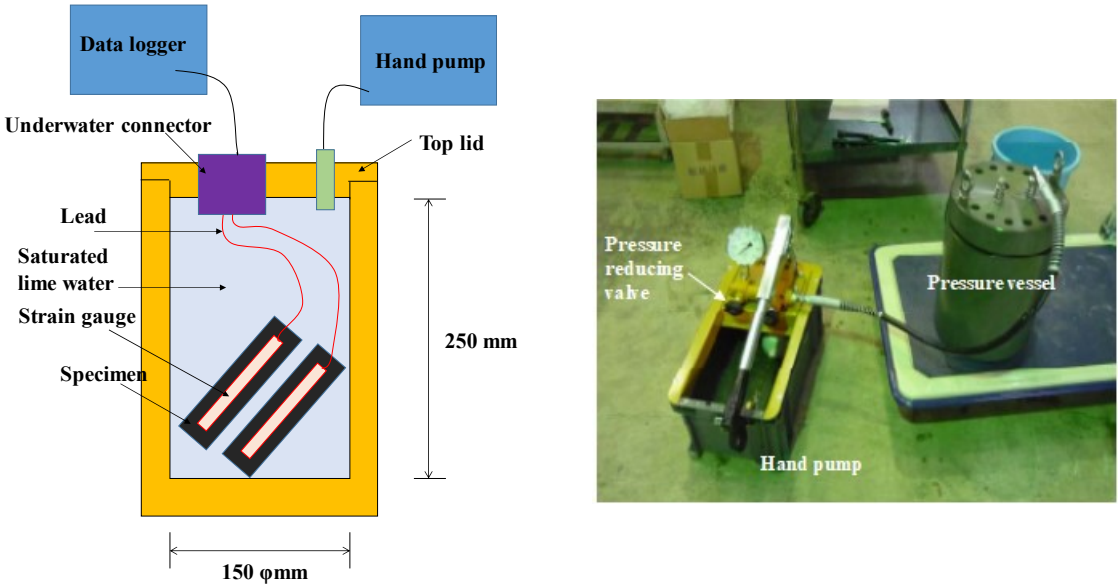

Fig. 3 Apparatus for the strain measurement of hardened specimens while under hydraulic pressure of 17 MPa.

day. The histogram of the brightness values obtained from the three-dimensional images as a function of the pressurization periods is shown in **Fig. 5**. The brightness values were averaged with 1504 slices. The gray level of each pixel represents a density value corresponding to the linear attenuation coefficient of the element contained in that pixel. There were two main peaks. The lower gray level (darker color: ca. 60–100) corresponds to pores. The peak with the higher gray level (around 110–180) is attributed to cement hydrates such as C-S-H. The peaks with the lower gray level became smaller when pressurized, which indicates that the pores were partially or fully saturated with liquid water with increasing periods of pressurization. After 30 min of pressurization, some pores close to the specimen surface could be saturated. Gray level at around 60–100 after 1 day was almost identical to that after 7 days, suggesting that almost all the pores were saturated with water after 1 day of pressurization. It should be noted that damage by short-term water infiltration was not observed in CT images. In fact, after depressurization, no crack was visible on the surface of the mortar specimen.

Figure 6 represents the strain while under 17 MPa of hydraulic pressure as a function of time. Contraction (compression) was considered to be a negative value. Applied hydraulic pressure was increased from atmospheric pressure to 17 MPa for the first 35 min. The strain decreased (specimen contracted) approximately linearly until the applied pressure reached 17 MPa, at which point the strain then increased (specimen was restoring to the original shape) gradually and returned to almost zero within 4 h, which can be provoked by water saturation of empty pores in the specimen. The strain remained about zero until 7 days elapsed, which indicated that creep had

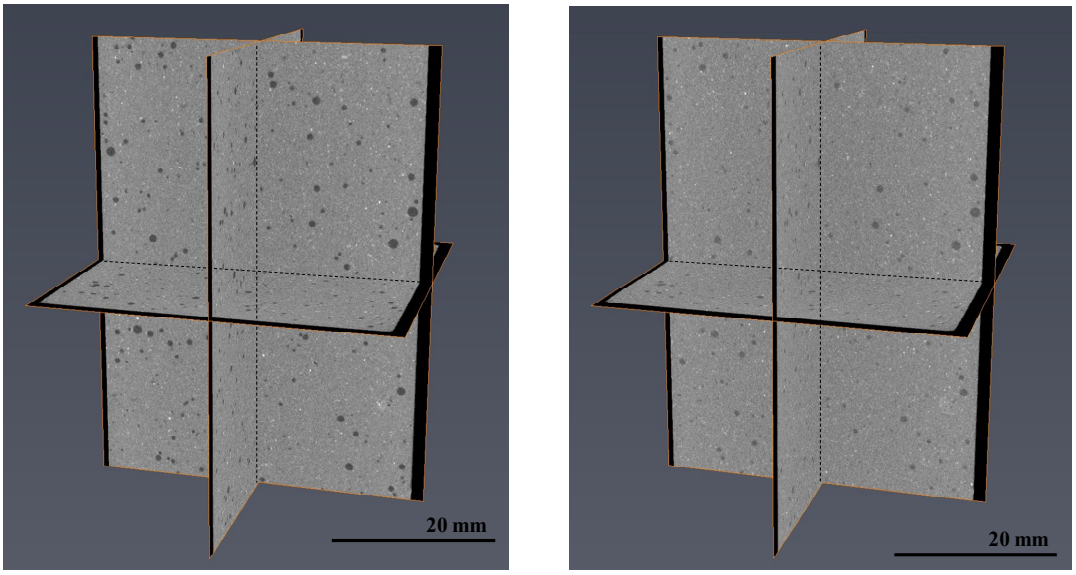

Fig. 4 Three-dimensional images of X-μCT scans of the mortar specimen before pressurization (*left*) and after pressurization for 1 day (*right*). Lower density point, e.g. empty pores that look darker in the image, have a smaller brightness value. Higher density point, e.g., water saturated pores and cement that look lighter in the image, have a higher brightness value.

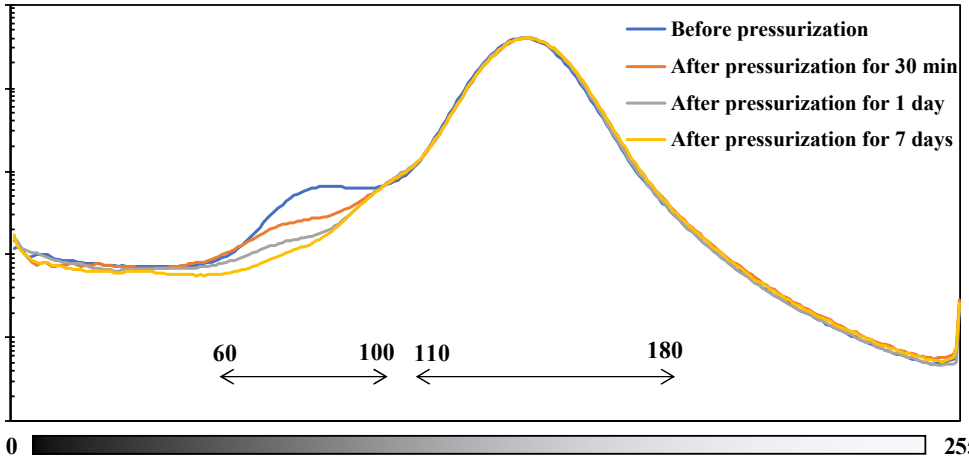

Fig. 5. Histogram of the brightness values for the three-dimensional images of each specimen. Brightness values were averaged with 1504 slices. The gray level at ca. 60–100 corresponds to pores, and ca. 110–180 is attributed to cement hydrates.

not occurred during this time period. Although the timing of the measurement is different, the result of the strain measurement is quite consistent with that of X-μCT (**Figs. 4** and **5**).

These results indicate that damages and dimensional changes at submillimeter to submicron scales as was reported in our previous study (Kobayashi *et al*. 2021) do not appear due to the action of short-term hydraulic pressure.

In addition, these results may be simply explained by the classic theory in the soil mechanics; the principle of effective stress by Terzaghi (1923). The effective stress $\boldsymbol{\sigma'}$ is related to total stress $\boldsymbol{\sigma}$ and the pore water pressure $\boldsymbol{u}$, as shown below.

$$\boldsymbol{\sigma} = \boldsymbol{\sigma'} + \boldsymbol{u} \tag{1}$$

Here, compression stress is assumed to be positive. From the macroscopic mechanics point of view, local effective stress acting on the skeleton $\boldsymbol{\sigma'}$ by the external water pressure $\boldsymbol{\sigma}$ is gradually increased before the liquid water infiltrates the mortar, which is a porous media, then released when liquid water is totally infiltrated into the mortar. At that time, the pore water is connected to the external water in the vessel, and the pore water pressure $\boldsymbol{u}$ is equal to the external pressure $\boldsymbol{\sigma}$, which means $\boldsymbol{\sigma'} = 0$ and no volumetric strain generates. In this experiment, the mortar with a water-to-cement ratio of 0.6 was used, so the microstructure was not relatively dense. Therefore, the liquid water easily infiltrated, leading to stress relaxation on the skeleton.

From the standpoint of this principle, the mortar specimen size may play a role: once water infiltration is delayed for large-scale specimens or dense specimens, the effective stress of the skeleton of any area that is not filled with liquid water should resist against the external total stress, possibly leading to damage development. On the contrary, the area where the liquid water has not infiltrated is under isotropic confinement, which increases the strength. Therefore, damages due to hydraulic pressure would strongly depend on the balance between the hydraulic pressure for stress development of the skeleton and the water infiltration for stress release of the skeleton.

(2) Pore volume, weight change, compressive strength and bending strength

Figure 7 represents incremental pore volume and cumulative pore volume of the mortar specimens before and after the hydraulic pressurization at 17 MPa. After pressurization for 1 day and subsequent depressurization, the pore volume of >70 nm in diameter increased slightly and the peak position of 40 nm in diameter before pres-

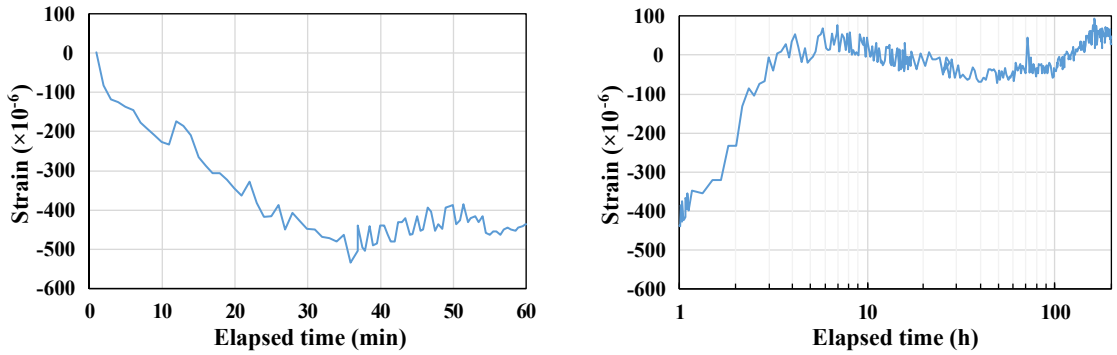

Fig. 6 Strain of the mortar specimen while under 17 MPa of hydraulic pressure as a function of time. (*left*: initial 60 min, *right*: from 1 h to 7 days).

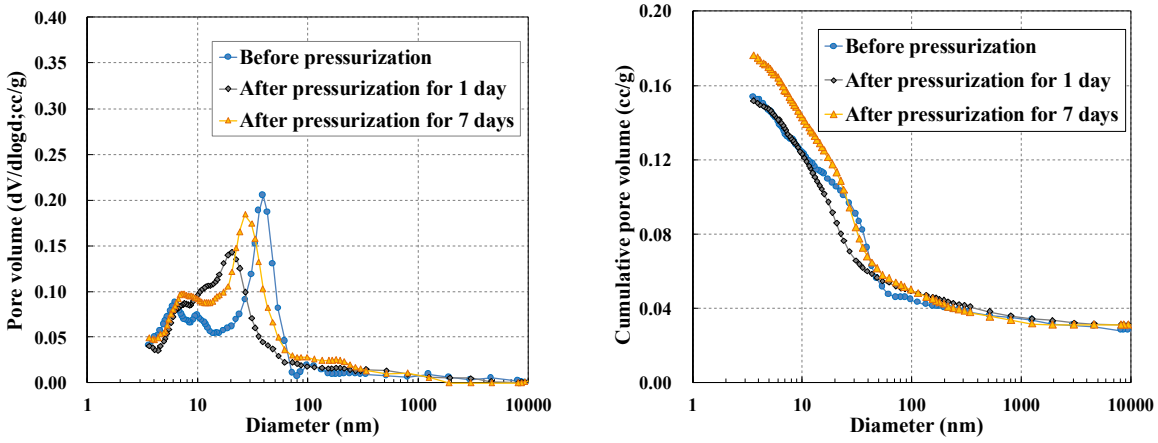

Fig. 7 Incremental pore volume (*left*) and cumulative pore volume (*right*) of the mortar specimens before and after the hydraulic pressurization at 17 MPa. dV/dlogd: dividing the differential pore volume (dV) by the logarithmic differential pore diameter (dlogd).

Table 4 Weight change, compressive strength and bending strength of the mortar specimens before and after the hydraulic pressurization at 17 MPa. Weight gain was considered a positive value. Measured data of 3 specimens were averaged.

	Weight change (%)	Compressive strength (N/mm^2)	Bending strength (N/mm^2)
Before pressurization	–	36.0	4.6
After pressurization for 1day	3.2	35.4	4.3
After pressurization for 7 days	3.3	33.1	4.4

surization was shifted to 20 nm in diameter after pressurization for 1 day. The loss of pore connectivity and the compressive damages on pores could be considered as a pore closure. The pores closed following 1 day of pressurization and subsequently reopened after 7 days of pressurization. These changes in pore-size distribution could be caused by the combination of water infiltration and confinement that could lead to the initial closing of the pores and the subsequent opening due to the differential release of external and internal pressures, as well as the release of the confining stress itself. As saturated lime solution was used in this measurement, pore opening cannot be attributed to decalcification of portlandite and C-S-H (Phung *et al*. 2016; Bossa *et al*. 2015). Further investigation will be necessary to clarify how this microstructural changes by the short-term hydraulic pressure affect the long-term durability and dimensional stability.

Table 4 shows weight change, compressive strength and bending strength of the mortar specimens before and after the hydraulic pressurization at 17 MPa. Water absorption of the mortar specimens increased the weight after 1 day of pressurization. The prolonged pressurization period did not result in changes in weight gain. Water uptake to the specimens can be cross-checked in **Figs. 4** and **5**, where water saturation in pores did not differ in the histogram of X-μCT between 1 day and 7 days. Compressive strength and bending strength after the pressurization for 1 day and 7 days were slightly decreased compared to before pressurization. The decrease in strength could be provoked by the water infiltration and confinement. Visible damages and cracks were not observed on the specimen after pressurization for 1 day and 7 days.

4. Challenging project: in-situ exposure test at 3515 m depth in Nankai Trough

As mentioned in Section 3, damages by the short-term hydraulic pressure can not be observed at submillimeter to submicron scales but some microstructural changes were shown, which might lead to durability concern. Authors have already started investigations to elucidate the effects of long-term and higher hydraulic pressure both at a laboratory scale and actual deep-sea field. A related progress of our challenging project is introduced in this section.

With the view toward deep-sea infrastructure construction, the authors have set up a project targeted creating a technology platform for the use of in-situ monitoring methods at deep ocean bottom sites and the corresponding evaluation of cement-based materials by the in-situ measurement apparatus. Our first in-situ trial measures the time dependence of volumetric stability and microstructure of a hardened cement mortar as a result of long-term exposure to the 3515-m deep seabed environment at Nankai Trough in the Pacific Ocean. Prior to the in-situ exposure test at Nankai Trough, the pressure that acted on the large mortar specimens and the strain were measured using a hyperbaric chamber.

Due to the limitation of experimenting opportunity, each measurement in this section was conducted once with one mortar specimen.

4.1 Project details

(1) Specimen

The mortar mix B shown in **Table 1** was used to prepare the cylindrical larger scale specimens. The water-to-cement ratio was 0.60 as well in 3.1. The dry mortar mix was pre-mixed and subsequently mixed with water for 3 min at 1100 rpm using a hand-held mechanical mixer. Then, the mortar was poured into a cylindrical mold with a 350-mm diameter base and a 400-mm height. This mold size allowed for four strain gauges PML-60 and three pressure gauges PWF-50MPB (Tokyo Measuring Instruments Laboratory Co, Ltd.) to be embedded as shown in **Fig. 8**. The head size of the pressure gauge was 14.8 mm in diameter and 51 mm in length. Strain gauges were also embedded midway lengthwise in the specimen: two centered along its axis perpendicular to each other and flanked also by one at 100 mm and one at 40 mm from the curved side surface of the specimen (positions described as 1/2r and 1/4r respectively). Pressure gauges were also embedded widthwise 80 mm from each base of the specimen, situated contiguous to the center, and at 1/2r and 1/4r. All cables were covered with waterproofing materials. The surface of the upper and lower bases of the cylindrical mortar specimen were coated with a water-impervious epoxy resin in order to monitor the effects of water infiltration from side surface.

Table 3 shows flow value, air content and density of the mortar B immediately after mixing, and compressive and bending strength of the mortar specimen cured for 28 days under sealed conditions. Both testing and curing were performed at a constant temperature of 20ºC 65% RH. Prior to the in-situ subsea exposure, the mortar specimen was cured for 28 days under the sealed condition at 20ºC. Variation of the temperature and humidity was ±1ºC and ±5 % RH, respectively.

(2) Ongoing in-situ exposure test and measurement apparatus

Our results represent that contraction occurs initially in the mortar specimen due to hydraulic confinement, and water infiltration could release the internal pressure and restore the specimen to its original shape, however, the effects of long-term hydraulic pressure have not been clarified. The in-situ subsea test being performed at 3515 m depth in Nankai Trough will reveal the creep behavior and the corresponding microstructure changes of the mortar specimen as well as synergistic effects between hydraulic pressure and cold seawater attack.

Figure 9 depicts the apparatus designed for in-situ measurements of strain and pressure on the seabed. The data logger TDS–150 (Tokyo Measuring Instruments Laboratory Co., Ltd.) was stored in a pressure resistant housing made of aluminum alloy. The inner vessel of this pressure resistant housing was 120 mm in diameter and 467.5 mm in length. Electric insulating polyimide film was pasted on the inner surface of the vessel in order to avoid energization due to the contact of the substrates to the inner surface caused by vibration during the diving. Strain and pressure gauges embedded in the mortar specimen were connected to the data logger via the underwater connector Subconn Circular BH25F and IL25M (MacArtney Co.) penetrating the lid of the pressure resistant housing.

The mortar specimen and the apparatus designed for in-situ measurements were set on the seabed at deep sea research site at 3515 m depth by the remotely operated vehicle ROV Kaiko MK–IV during the KR 20-07 cruise. **Figure 10** shows the ROV Kaiko MK-IV and its basket where the mortar specimen and the apparatus were loaded. The deep sea experimental field is located at the northern edge of Nankai Trough off Sagami Bay in Japan, N34°1.65’ E138°31.50’ as pointed out in **Fig. 11**. The temperature, salinity and dissolved oxygen of seawater at the experimental site were constant at 1.5ºC, 35 PSU and 3.1 mL/L, respectively. Operations were monitored by the camcorder equipped onboard the ROV. **Figure 12** depicts the mortar specimen and the apparatus during the diving operation to the research field. The diving speed of Kaiko MK–IV was ca. 50 m/min, which was equivalent to a pressurization rate of 0.5 MPa/min. The installation operation of the mortar specimen and the apparatus onto a frame at the deep sea research site by using a manipulator of the ROV Kaiko MK-IV is shown in **Figs. 13** and **14**. The in-situ test began on August 25th in 2020, and the specimen and apparatus will be salvaged in 2021.

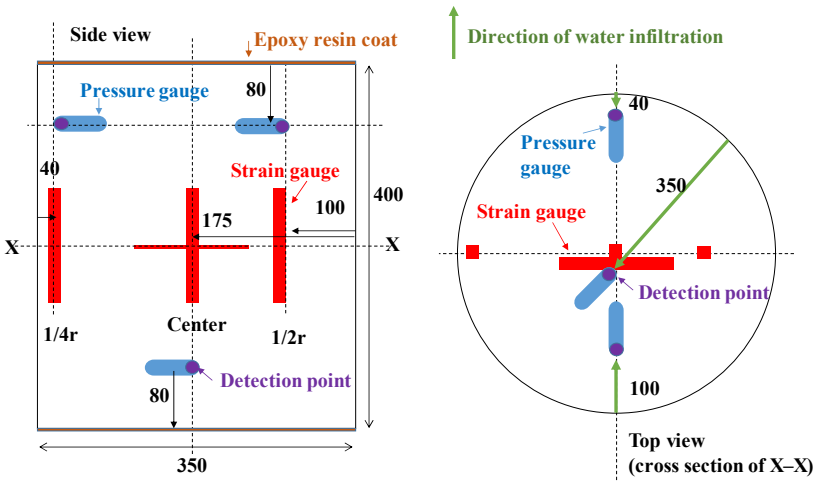

Fig. 8 Schematic of the embedded strain (*red*) and pressure gauges (*blue*) in the cylindrical mortar specimen (unit: mm).

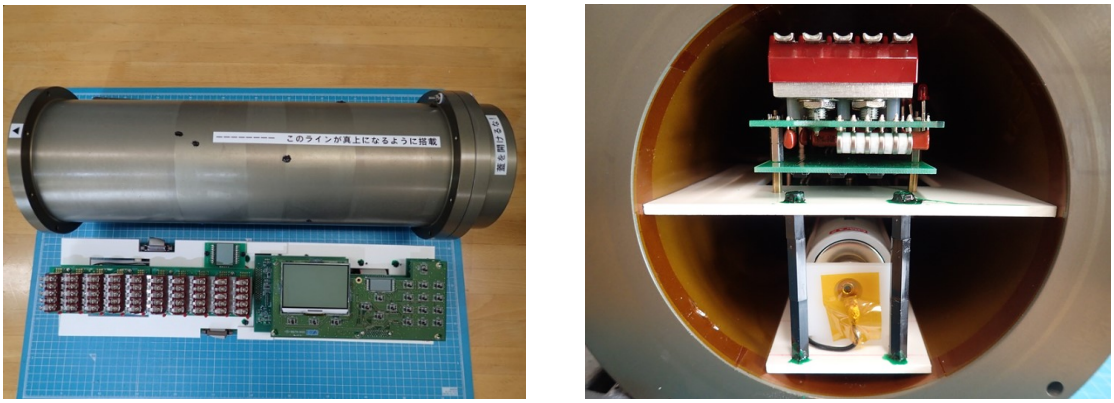

Fig. 9 Apparatus designed for in-situ deep sea measurements of strain and pressure. Data logger TDS–150 was stored in a pressure resistant housing made of aluminum alloy.

(3) Testing results under 35 MPa of hydraulic pressure using a hyperbaric chamber

A preliminary testing was conducted to measure the pressure exerted on the mortar specimen and strain while under 35 MPa of hydraulic pressure using a hyperbaric chamber possessed by Japan Agency for Marine-Earth Science and Technology (JAMSTEC), which is related to the ongoing in-situ exposure test. The effective dimension of the inner vessel of the hyperbaric chamber was 600 mm in diameter and 1600 mm in height. The inner vessel was filled with tap water. Both pressurization and depressurization rates were auto-controlled at 0.6 MPa/min, which simulates diving and salvaging speeds of the remotely operated vehicle (ROV) Kaiko MK-IV used for the in-situ exposure test. The pressure was increased from 0.1 MPa to 35 MPa and then kept constant at 35 MPa for 3 h, followed by a decrease to 0.1 MPa. Strain gauges and pressure gauges embedded in the mortar specimen were connected to a data logger via an underwater connectors Subconn Circular BH25F and IL25M, penetrating the top lid of the hyperbaric chamber. Strain and pressure were measured continuously during the 5 h from the start of applying hydraulic pressure. The measured strain and pressure values were corrected for the length and cross-sectional area of the extended lead.

Figure 15 shows the changes in strain and pressure in the mortar specimen while under hydraulic pressure using the hyperbaric chamber. Strain decreased (the specimen contracted) linearly due to water confinement as the applied hydraulic pressure increased at a constant

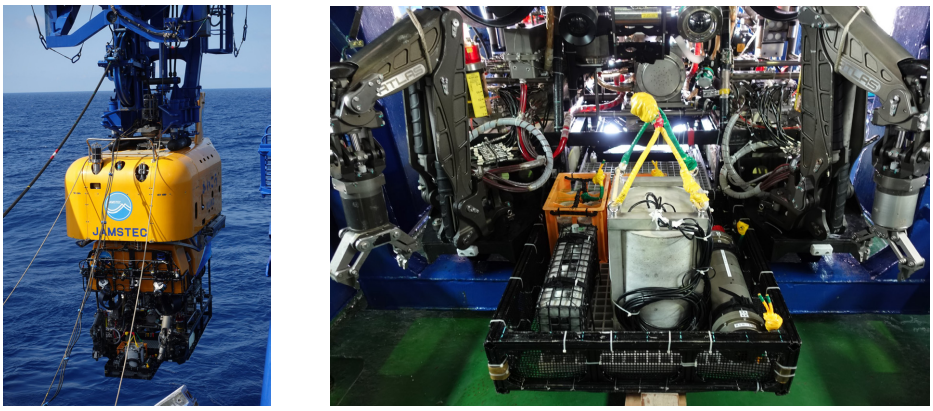

Fig. 10 The ROV Kaiko MK–IV (*left*) and mortar specimen and the apparatus designed for in-situ measurements loaded in the basket of the ROV Kaiko MK-IV (*right*) during the KR 20-07 cruise.

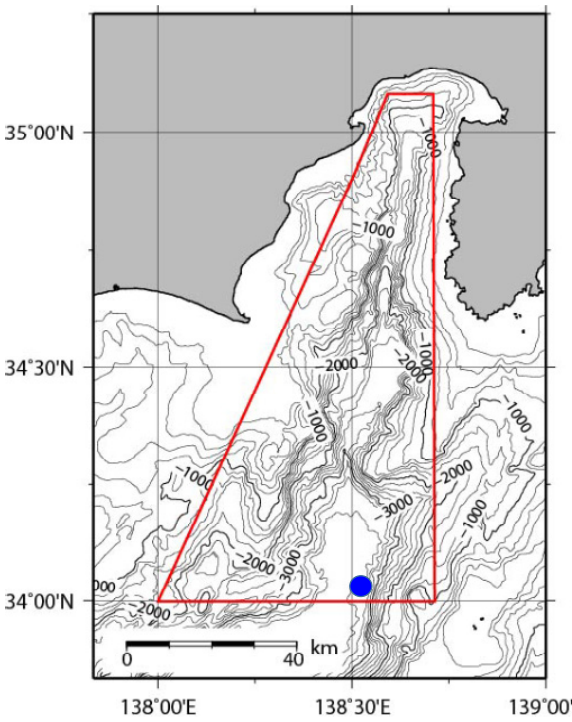

Fig. 11 Nautical chart of northern edge of Nankai Trough off Sagami Bay in Japan (*within red frame*), and installation point N34°1.65' E138°31.50 (*blue point*).

Fig. 12 Mortar specimen and apparatus for in-situ measurement during the dive to the deep sea experimental field location at Nankai Trough.

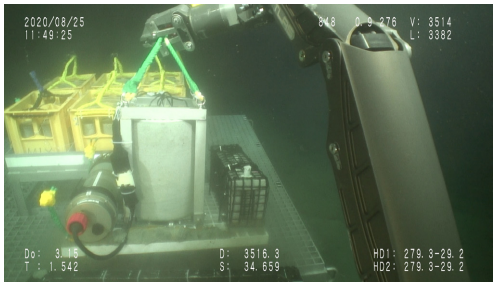

Fig.13 Operation using a manipulator of the ROV Kaiko MK–IV to install the mortar specimen and the apparatus onto the frame at the deep sea test field on the ocean floor.

rate of 0.6 MPa/min. At 1/4r, pressure was detected 10 min after the start and became equivalent to the applied hydraulic pressure after 45 min. The pressure at 1/2r was generated at 40 min after the start and became equivalent to the applied hydraulic pressure at ca. 3 h. The pressure at the center was generated after 3 h from the start but the measurement was ended before the pressure reached the point equivalent to the applied hydraulic pressure. These results could be interpreted as follows: once liquid water reached approximately the detection point of the embedded pressure gauge, the pressure value started to increase. The pressure value became equivalent to the applied hydraulic pressure when the gauge's detection point was saturated with infiltrated liquid water (stress relaxation on the skeleton).

When the applied hydraulic pressure reached 35 MPa at 1 h after pressurization, approximately –1600 to –1800 μ of strain was observed at each part of the specimen. After 1 h from the start, the strain increased (the specimen was restoring to the original shape) at the center as well as at 1/2r and 1/4r. Although the pores at the center and 1/2r could not have been fully saturated with water, some internal pressure could be released due to water saturation of empty pores closer to the curved side surface of the specimen. Compared to the center, the increase of strain became pronounced at 1/4r and 1/2r, which are closer to the side surface of the specimen. Strain values measured with the gauges embedded lengthwise in the specimen had settled at ca. –700 μ after approximately 4 h elapsed.

A sharp "bump", a sudden decrease, appeared in the pressure curve of 1/2r after ca. 3 h elapsed. This bump could indicate the generation of negative pressure due to pronounced pore opening and/or cracking near the detection point of the pressure gauge. When water flowed into that point where the negative pressure acted, the once-dropped pressure could return to the pressure reached before the pore opening and/or crack initiation. Another sharp bump, however, a sudden increase, was observed in the pressure curve of the center after ca. 4 h elapsed. Although the reason for this abrupt increase has not been identified, it noticeably coincided with the start of depressurization process.

Figure 16 depicts a photo of the specimen taken after the depressurization process. Cracks appeared along the

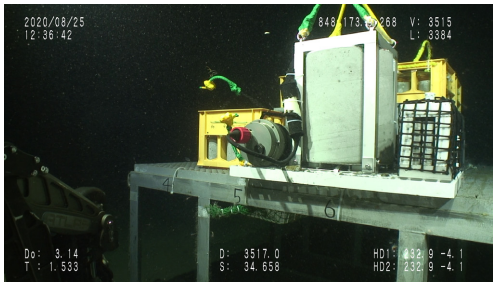

Fig. 14 Completed installation of the mortar specimen and the apparatus on the frame of the deep sea test field.

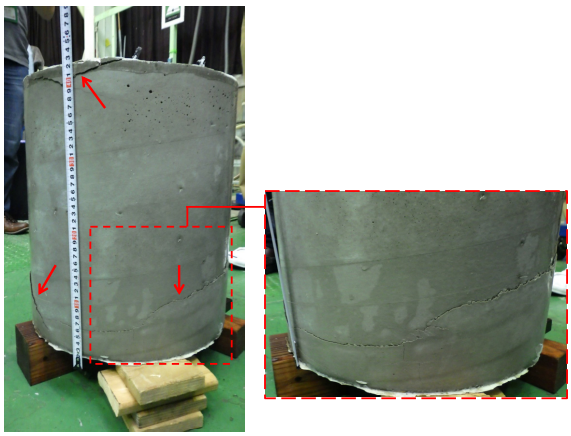

Fig. 16 A photo of the mortar specimen taken after the depressurization process shows cracks (marked with a red arrow) appeared along the curved side of cylindrical surface nearing the upper and lower circular bases.

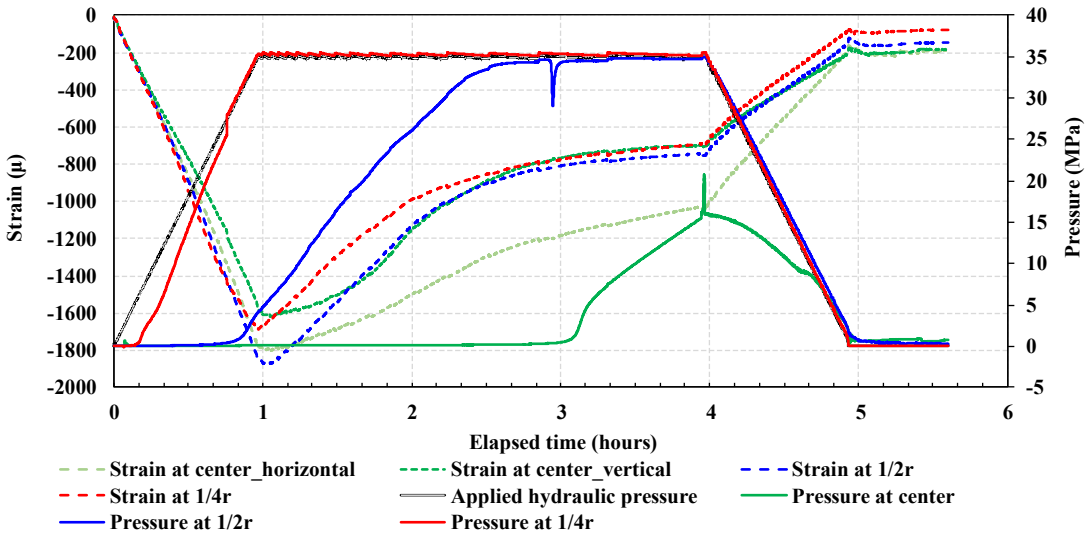

Fig. 15 A preliminary test to simulate the deep-sea exposure. Changes in strain and pressure act on the mortar specimen while under hydraulic pressure using the medium-sized hyperbaric chamber.

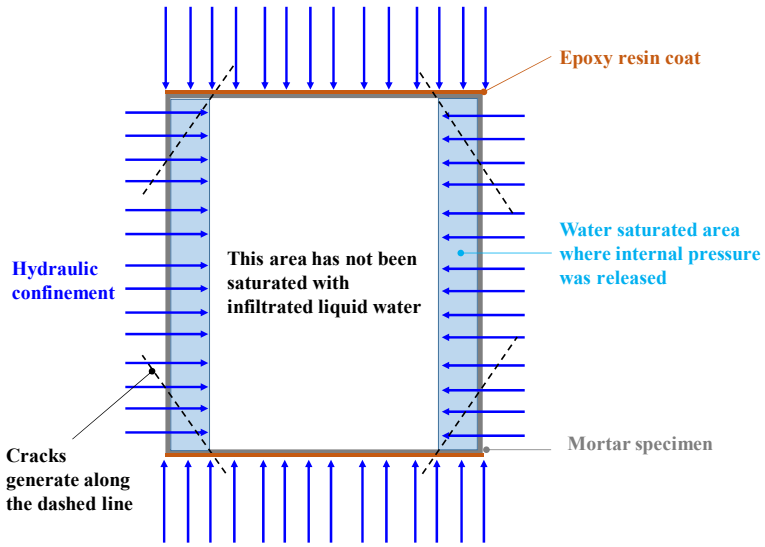

Fig. 17. An image of crack generation due to the balance between the release of internal pressure in the specimen and 3-axis hydraulic confinement of the specimen.

curved side surface near the surfaces of the upper and lower bases of the specimen and could possibly extend inside the specimen as illustrated in **Fig. 17**. As liquid water could infiltrate only from the side surfaces, portions of the water saturated area, where internal stress on the solid skeleton was released, could not be balanced with hydraulic confinement (external stress), and therefore, cracks were generated diagonally from the upper and lower base surfaces toward the curved side surface. This damage on the specimen could be indicating the size effect as mentioned in 3.4 (1).

5. Conclusion and outlook

Our quest to utilize cement-based materials in the special extreme environment, the deep sea, has just begun. Considerable research and development that will focus on material designs, structure designs and construction methods will be necessary to build and maintain underwater deep-sea infrastructures. Our first trials focused on the action of hydraulic pressure at a laboratory scale brought the following observations:

(1) Initial damages by short-term water infiltration and confinement were less visible by X-μCT,
(2) Mortar specimen contracted due to the initial water confinement, then appeared to return to the original shape within a few hours due to the water saturation in empty pores that leads to the release of internal stress on the skeleton. However, time dependence such as creep behavior neither appeared during the first 7 days of the laboratory test using small-scale specimen, nor the first 4 h of the test using the large-scale specimen in the hyperbaric chamber,
(3) Through pressurization and depressurization processes, weight gain, changes in pore-size distribution and slight decrease in strength were observed.

These findings indicate that the action of short-term hydraulic pressure could not be a direct factor deteriorating the mortar specimens as reported in our previous study – significant disintegration of the mortar specimens exposed to deep-sea environment at Tarama Knoll. Microstructural changes by the short-term pressurization might affect the long-term durability and volumetric stability. Therefore, further investigations will be necessary to elucidate the effects of long-term and higher hydraulic pressure.

The first-ever in-situ test in deep-sea environments with a view to investigating the time dependence of changes in volume fraction, microstructure and synergistic effects between hydraulic pressure and cold seawater attack due to the long-term exposure to deep ocean bottom conditions is currently being performed at a 3515-m depth in the Nankai Trough. Results of the in-situ measurement and the corresponding discussion will be published soon.

Acknowledgements

We would like to thank Professor Toshiro Yamanaka and Associate Professor Hiroko Makita at Tokyo University of Marine Science and Technology for useful discussions. We thank Dr. Daiki Takano at Port and Airport Research Institute for performing the image processing of X-μCT.

References

Albertsen, N. D., (1973). "*Influence of compressive strength and wall thickness on behavior of concrete cylindrical hulls under hydrostatic loading* (TR R-790)." Technical Report of Civil Engineering Laboratory, Port Hueneme, CA: Naval Construction Battalion Center.

Araki, E., Saffer, M., Kopf, A. J., Wallace, L. M., Kimura, T., Machida, Y., Ide, S., Davis, E. and IODP Expedition 365 shipboard scientists., (2017). "Recurring and triggered slow-slip events near the trench at the Nankai Trough subduction megathrust." *Science*, 356, 1157-1160.

Bossa, N., Chaurand, P., Vicente, J., Borschneck, D., Levard, C., Aguerre-Chariol, O. and Rose, J., (2015). "Micro- and nano-X-ray computed tomography: A step forward in the characterization of the pore network of a leached cement paste." *Cement and Concrete Research*, 67, 138-147.

Clayton, N., (1998). "Effect of water pressure on concrete strength." In: O. Gjorv, O., Sakai, K. and Banthia, N., Eds., *The 2nd International Conference on Concrete under Severe Conditions*, Tromsø, 978-987.

Craig, H., Broecker, W. S. and Spencer, D., (1981). "*GEOSECS Pacific expedition*." Vol. 4, Sections and profiles, U.S. Government Printing Office.

Danovaro, R., Corinaldesi, C., Dell'Anno, A. and Snelgrove, P. V. R., (2017). "The deep-sea under global change." *Current Biology*, 27(11), R461-R465.

De Weerdt, K., Justnes, H. and Geiker, M. R., (2014). "Changes in the phase assemblage of concrete exposed to sea water." *Cement and Concrete Composites*, 47, 53-63.

Gjorv, O. E., (1971). "Long-time durability of concrete in seawater." *ACI Journal*, 68(10), 60-67.

Hampel, E., Speck, K., Scheerer, S., Ritter, R. and Curbach, M., (2009). "High performance concrete under biaxial and triaxial loads." *ASCE Journal of Engineering Mechanics*, 135(11), 1274-1280.

Haynes, H. H., Highberg, R. S. and Nordby, B. A., (1976). "Seawater absorption and compressive strength of concrete at ocean depths (N-1436)." *Technical note of Naval Civil Engineering Laboratory*, Port Hueneme, California: Naval Construction Batallion Center.

Haynes, H. H. and Rail R. D., (1986). "*Handbook for design of undersea, pressure-resistant concrete structures*." Port Hueneme, California: Naval Civil Engineering Laboratory.

Hori, T., Chijiwa, N. and Iwanami, M., (2015). "A fundamental research on fracture behavior of concrete under high water pressure." *Journal of Japan Society of Civil Engineers, Series B3*, 71(2), I-179-I-184.

Hume, D., (2018). "Ocean storage of CO_2." *The Maritime Executive* [online], Available from: <https://www.maritime-executive.com/index.php/features/ocean-storage-of-co2> [Accessed 11 Feb 2021].

Jakobsen U. H., De Weerdt, K. and Geiker, M. R., (2016). "Elemental zonation in marine concrete." *Cement and Concrete Research*, 85, 12-27.

JAMSTEC, (n.d.). "*Medium sized hyperbaric chambers*." [online], Available from: <http://www.jamstec.go.jp/e/about/equipment/yokosuka/chugata_kouatsu_jikken.html> [accessed 11 Feb 2021].

JAMTEC, (2017). "*Yokosuka cruise report* (YK17-17)." Available from: <http://www.godac.jamstec.go.jp/catalog/doc_catalog/metadataDisp/YK17-17_all> [accessed 11 Feb 2021].

Kobayashi, M., Takahashi, K. and Kawabata, Y., (2021). "Physicochemical properties of the Portland cement-based mortar exposed to deep seafloor conditions at a depth of 1680 m." *Cement and Concrete Research*, 142, 106335.

Le Breton, R., (2019). "KM3NeT: Next-generation neutrino telescope in the Mediterranean Sea." *Nuclear Instruments and Methods in Physics Research Section A: Accelerators, Spectrometers, Detectors and Associated Equipment*, 936, 204-207.

Mather, B., (1964). "Effects of sea water on concrete." In: *Highway Research Board -Highway Research Record*, 33-42.

Margiotta, A., (2014). "Status of the KM3NeT." *Journal of Instrumentation*, 9(4), C04020.

Mander, J. B., Priestley M. J. N. and Park, R., (1988). "Theoretical stress-strain model for confined concrete." *Journal of Structural Engineering*, 114(8), 1804-1826.

Mehta, P. K., (1990). "*Concrete in the Marine Environment.*" New York: CRC Press.

Miller, K. A., Thompson, K. F., Johnston, P. and Santillo, D., (2018). "An overview of seabed mining including the current state of development, environmental impacts, and knowledge gaps." *Frontiers in Marine Science*, 4, 418.

Mohammed, T. U., Hamada, H. and Yamaji, T., (2003). "Marine durability of 30-year old concrete made with different cements." *Journal of Advanced Concrete Technology*, 1(1), 63-75.

Pauli, D. C. and Clapper, G. P., eds., (1967). "*Project SEALAB report – an experimental 45-day undersea saturation dive at 205 feet – SEALAB II project group* (ONR report, ACR-124)." Technical Report of Office of Naval Research Department of the Navy, Washington DC: Office of Naval Research.

Phung, Q. T., Maes, N., Jacques, D., De Schutter, G. and Ye, G., (2016). "Investigation of the changes in microstructure and transport properties of leached cement pastes accounting for mix composition." *Cement and Concrete Research*, 79, 217-234.

Ports and Harbours Bureau, National Institute for Land and Infrastructure Management, and Port and Airport Research Institute, MLIT., (2009). "*Technical standards and commentaries for port and harbor facilities in Japan* (Part II, Chapter 11)." Tokyo: The Overseas Coastal Area Development Institute of Japan, 338-341.

Rail, R. D., Wendt, R. L. and Naval Civil Engineering Laboratory, (1985). "*Long-term deep-ocean test of concrete spherical structures – Results after 13 years* (NCEL Technical Report R–915)." Port Hueneme, California: Naval Civil Engineering Laboratory, 65.

Ramirez, L. E. and Billet, D. S. M., (2006). "Deep-sea ecosystems: pristine biodiversity reservoir and technological challenges." In: C. M. Duarte, Ed. *The Exploration of marine biodiversity, scientific and technological challenges*. Bilbao, Spain: Fundacion BBVA, 63-92, 154pp.

Ritter, R. and Curbach, M., (2015). "Material behavior of ultra-high-strength concrete under multiaxial stress states." *ACI Material Journal*, 112, 5, 641-651.

ROBEX, (n.d.). "*ROBEX - Robotic Exploration of Extreme Environments*." Available from: <https://www.robex-allianz.de> [Accessed 11 Feb 2021].

Sakai, T., Inoue, K., Watanabe, H., Mcdonough, W. F., Ueki, K., Abe, N., Sakurai, N., Kyo, M., Araki, E., Kasaya, T. and Yoshida, H., (2020). "Study of ocean bottom detector for observation of geo-neutrinos from mantle." In: *Japan Geoscience Union – American Geophysical Union Joint Meeting 2020*, U20-P01.

Sharma, R., (2015). "Environmental issues of deep-sea mining." *Procedia Earth and Planetary Science*, 11, 204-211.

Shimizu Corporation, (n.d.) "*Ocean spiral – Deep sea future city concept*." Available from: <https://www.shimz.co.jp/en/topics/dream/content01/> [Accessed 11 Feb 2021]

Terzaghi, K., (1923). "Die Berechnung der Durchlässigkeitsziffer des Tones aus dem Verlauf der hydrodynamischen Spannungserscheinungen." *Akademie der Wissenschaften in Wien, Sitzungsberichte, Mathematisch-naturwissenschaftliche Klasse, Abteilung*, II a. 132, 105-124. (in German)

Wang, Q., Liu, Y. and Peng, G., (2016). "Effect of water pressure on mechanical behaviour of concrete under dynamic compression state." *Construction and Building Materials*, 125, 501-509.

Wilhelm, S. and Curbach, M., (2017). "Experimental and nonlinear numerical analysis of underwater housings for the deep sea, made of ultra-high performance concrete." *Structural Concrete*, 18, 216-224.